Snow reconciles observed and simulated phase partitioning and increases cloud feedback

Grégory V. Cesana[1,2], Andrew S. Ackerman[2], Ann M. Fridlind[2], Israel Silber[3] and Maxwell Kelley[2]

[1] Center for Climate Systems Research, Columbia University, New York, NY

[2] NASA Goddard Institute for Space Studies, New York, NY

[3] Pennsylvania State University, University Park, PA

Corresponding author: Grégory V. Cesana (gregory.cesana@columbia.edu)

Key Points:

- Accounting for snow in a lidar simulator to compare with observations systematically reduces the simulated apparent supercooled liquid
- Allowing radiative schemes to be snow-aware in climate models greatly increases their net cloud feedback
- The mean climate sensitivity is greater for recent CMIP models with snow-aware radiative schemes compared to those without

Abstract

The surprising increase of Earth's climate sensitivity in the most recent Coupled Model Intercomparison Project (CMIP) models has been largely attributed to extratropical cloud feedback, which is thought to be driven by greater supercooled water in present-day cloud phase partitioning (CPP). Here we report that accounting for precipitation in the Goddard Institute for Space Studies ModelE3 radiation scheme, neglected in more than 60% of CMIP6 and 90% of CMIP5 models, systematically changes its apparent CPP and substantially increases its cloud feedback, consistent with results using CMIP models. Including precipitation in the comparison with Cloud–Aerosol Lidar and Infrared Pathfinder Satellite Observations (CALIPSO) measurements and in model radiation schemes is essential to faithfully constrain cloud amount and phase partitioning, and simulate cloud feedbacks. Our findings suggest that making radiation schemes precipitation-aware (missing in most CMIP6 models) should strengthen their positive cloud feedback and further increase their already high mean climate sensitivity.

Plain Language Summary

The surprising increase of Earth's climate sensitivity – a proxy for future global warming – in the most recent climate models (CMIP6) has been largely attributed to the response of extratropical low clouds to warming. This cloud-climate feedback is thought to be driven by greater supercooled water in present-day cloud phase partitioning. Here we report that accounting for precipitation in climate model radiation schemes –neglected in more than 60% of CMIP6 and 90% of CMIP5 models– profoundly changes their apparent cloud phase partitioning and substantially increases their cloud-climate feedbacks, which has not been reported before. Including precipitation in the comparison with observations and in model radiation schemes is essential to faithfully constrain cloud amount and phase partitioning and simulate cloud-climate feedbacks. Our novel findings suggest that making radiation schemes precipitation-aware, which is missing in most CMIP6 models, should strengthen their positive cloud feedback and further increase their already high mean climate sensitivity

1. Introduction

Whether clouds are composed of liquid droplets, ice crystals, or a mixture of both at supercooled temperatures (between the melting point and the temperature at which cloud droplets freeze homogeneously, circa -40˚C) is of particular interest since liquid and frozen hydrometeors generally have distinct radiative properties. For a given condensed water content, liquid clouds are typically more opaque than their frozen counterparts, which results in stronger reflection of shortwave (SW) radiation and also more absorption and emission of longwave (LW) radiation for a given water content at the same temperature (e.g., Cesana and Storelvmo, 2017; Mülmenstädt et al., 2021; Tsushima et al., 2006).

In a warmer climate, it is expected that more supercooled droplets would form at the expense of ice crystals (e.g., Mitchell et al., 1989), thereby reducing other supercooled droplet sink processes (e.g., Wegener-Bergeron-Findeisen process; Korolev, 2007), and fewer droplets would be converted to precipitation (e.g., Ceppi et al., 2016). Therefore, more water clouds would persist, increasing average optical depth and cloud lifetimes (e.g., Cesana and Storelvmo, 2017; Mülmenstädt et al., 2021; Senior and Mitchell, 1993). As a result, the amount of SW radiation reflected back to space would be increased, thereby reducing the initial surface temperature warming through a negative feedback, widely referred to as the cloud optical depth feedback. Among cloud feedbacks, a reduction in the optical depth feedback produced by low-level clouds (at heights ≤ 3 km) in the extratropics is thought to explain most of the increase in equilibrium climate sensitivity (ECS; a measure of the surface air temperature increase from a hypothetical abrupt doubling of CO_2 concentrations) between simulations from the Coupled Model Intercomparison Project (CMIP) phase 5 and 6 Earth system models (ESMs) (Zelinka et al., 2020).

The strength of this optical depth feedback is tightly connected to how cloud phase is partitioned in ESMs, referred to as cloud phase partitioning (CPP) and the amount of ice in the historical climate (e.g., Tsushima et al., 2006). One way to describe the CPP is the supercooled cloud fraction (Tan et al., 2016) (SCF), a quantity that is often underestimated in ESMs compared to observations (Cesana et al., 2012, 2015; Cesana and Chepfer, 2013; Komurcu et al., 2014; Quaas, 2004). Consequently, considerable attention has been paid to increasing the amount of supercooled condensates in the latest ESMs. In contrast, larger hydrometeors, typically snow and rain classified in microphysics schemes as "precipitation", which are represented in all models, are often neglected in ESM radiation schemes although they are optically and radiatively relevant hydrometeors (Li et al., 2020). For example, while Hill et al. (2018) found that the radiative effect of rain may be small in climate models, Li et al. (2020) reported a substantial impact of snow on top-of-the-atmosphere (TOA) radiation fluxes as well as the radiative cooling in the atmosphere. An increasing number of ESMs now account for precipitation in their radiation schemes (Cesana et al., 2019; Gettelman and Morrison, 2015; Zhang et al., 2019), which raises the question of the extent to which precipitation can influence the CPP and subsequently the optical depth feedback, and ultimately the climate sensitivity.

CALIPSO observations provide liquid and ice cloud frequencies (Cesana et al., 2016; Hu et al., 2009; Yoshida et al., 2010) that are widely used to directly constrain ESM mass fractions of water and ice clouds (Kawai et al., 2019; Komurcu et al., 2014; Madeleine et al., 2020; McCoy et al., 2015; Tan et al., 2016). A direct comparison between an observed frequency of SCF and a simulated mass SCF would neglect important differences in the definition of observed and simulated cloud phase, as well the CALIPSO lidar instrument limitations (Cesana and Chepfer, 2013). Using a lidar simulator (Cesana et al., 2012; Cesana and Chepfer, 2013; Kay et al., 2016), which mimics what a CALIPSO-like lidar would observe over an ESM atmosphere, can offer a more accurate model evaluation. However, all hydrometeors can affect the CALIPSO lidar signal and increase the lidar cloud fraction regardless of whether they are considered cloud or precipitation in ESMs. As a result, the observed and simulated lidar cloud fractions correspond to the sum of cloud and precipitation fractions. However, many models do not account for precipitation in their radiation scheme and therefore do not pass on its contribution to the lidar simulator, making their lidar simulated cloud fractions a cloud-only fraction as opposed to a cloud and precipitation fraction. This difference has notable implications for comparisons of simulations and observations, and in turn for constraining the CPP.

2. Data and Methods

2.1. Observations

We use the GCM-Oriented CALIPSO Cloud Product (CALIPSO-GOCCP) cloud phase observations (Cesana et al., 2016; Cesana and Chepfer, 2013) that provide 333 m along-track-resolution near-nadir lidar profiles for 480 m height intervals. CALIPSO-GOCCP utilizes the state of lidar beam polarization to distinguish between ice and liquid-bearing clouds. A nonspherical ice crystal changes the polarization state of the lidar return contrary to a spherical droplet. However, the noise generated by highly reflective layers may complicate the distinction between the two water phases, in which case a pixel may be classified as “undefined phase”, which often correspond to mixed-phase clouds at subzero temperatures (Cesana et al., 2016). Regardless of their size, all hydrometeors may affect the lidar attenuated backscatter signal, including precipitation, although there is no distinction between precipitating and non-precipitating hydrometeors in CALIPSO-GOCCP cloud and cloud phase diagnostics. The main limitation of CALIPSO-GOCCP is related to lidar attenuation, which is full when the optical thickness of the atmosphere is greater than 3 to 5 (typically for thick cirrus clouds or dense liquid clouds) and may cause misdiagnosis of fully attenuated pixels as being clear sky and subsequent underestimation of the vertical cloud fraction near the surface (below 1 km, Cesana et al., 2016). However, this limitation and underestimation are reproduced in the simulations through the use of the lidar simulator. The observational uncertainty estimates used in this study, which are described further in the supplementary text S1, are derived from two sources of possible errors: error estimates from a CALIPSO-GOCCP evaluation study using *in situ* aircraft measurements (Cesana et al., 2016) and an error estimate based on the undefined-phase clouds, which can be considered as being either all liquid or all ice.

2.2. Model simulations

In this study, we primarily analyze monthly outputs from global simulations with prescribed sea surface temperatures (SST; following the Atmospheric Model Intercomparison Project, AMIP) from one of the four configurations of the latest version of the National Aeronautics and Space Administration Goddard Institute for Space Studies ModelE version 3 ESM (Cesana et al., 2019), referred to as GISS-ModelE3. Compared to the three other configurations, in which only cloud-related parameters are varied and not parameterization formulations, this configuration uses a variant model physics parameterization and best represents the CPP and high-level cloud amount compared to CALIPSO-GOCCP. Results from the other configurations are provided in the supplementary material. For the simulations without precipitation used in the section 3.4, we remove the effect of the large-scale frozen precipitation (snow) from the model radiation scheme while the physics of the model remain unchanged. We note that doing so negligibly impacts net radiative balance at TOA. These two setups, which are similar to Li et al. (2014a, 2014b), are representative of the two categories of CMIP models: those that do and do not account for precipitation in radiation calculations, although all treat moisture transport by precipitation. The GISS-ModelE3 configuration used in this study is based on the developmental version used in Cesana et al. (2019) further described in supplementary text S2.

2.3. Lidar simulator

To ensure a fair evaluation that accounts for the CALIPSO lidar limitations and uses similar cloud and cloud phase definitions and resolutions as in the observations, we use the CALIPSO-like outputs from GISS-ModelE3, obtained through the use of the CALIPSO lidar simulator (Cesana and Chepfer, 2013), to compare with the CALIPSO-GOCCP observations (Cesana et al., 2016; Cesana and Waliser, 2016). The lidar simulator computes lidar attenuated backscatter profiles using temperature, pressure, and water content and effective radius of cloud particles (Chepfer et al., 2008). A stochastic subcolumn generator is also used to characterize subgrid-scale variability and accounts for the model-specific overlap assumptions (Webb et al., 2001). When the lidar simulator was designed (Chepfer et al., 2008), it was decided to ignore the contribution of precipitation in the lidar signal return because most ESMs did not account for precipitation in their radiation scheme, which is no longer true (e.g., GISS-ModelE3, Cesana et al., 2019; the Community Earth System Model version 2, Danabasoglu et al., 2020; the Energy Exascale Earth System Model version 1, Golaz et al., 2019; see Table S3 for the full list). For this reason, we extended the lidar simulator used in GISS-ModelE3 by adding the contribution of all types of precipitation that are seen by the GISS-ModelE3 radiation code, i.e., stratiform snow and rain and convective snow, graupel and rain. As such, the modified lidar simulator is more consistent with CALIPSO-GOCCP observations, since the CALIPSO lidar signal is also affected by precipitating hydrometeors. In the lidar simulator, the parameterization of the backscatter-to-extinction ratio was built using particles with effective radius smaller than 70 micron (Chepfer et al., 2007, their Fig. 9). However, the parameterization is relatively stable for larger particles, which is why we use this particle size in the parameterization for all particles larger than 70 micron while we use the real particle size for the computation of the lidar extinction, which is sensitive to the particle size. Additionally, we modified a few other elements of the lidar simulator to make it more consistent with GISS-ModelE3, as described in supplementary text S3.

3. Results

3.1. Single Column Model case studies

We first use two single column model (SCM) case studies to evaluate the inclusion of precipitation in the lidar simulator and the ability of the lidar simulator to detect precipitation under realistic conditions. For this purpose, we use GISS-ModelE3 and the aforementioned modified version of the CALIPSO lidar simulator, which, like the model’s radiative transfer scheme, accounts for the effects of precipitation on our observational constraint of present-day cloud fraction and CPP. It is important to note that GISS-ModelE3 explicitly, compared to other GISS-

ESMs, explicitly represents supercooled cloud processes and precipitation, which are prognosed rather than diagnosed.

The first case represents a supercooled mixed-phase cloud that is continuously precipitating ice crystals and drizzle (Silber et al., 2019), a common occurrence over polar regions (Rangno and Hobbs, 2001; Silber et al., 2020), which ESMs typically struggle to reproduce (Klein et al., 2009). Roughly an hour after cloud formation, ice particles forming within the supercooled layer become visible and continue to grow as they fall through ice-supersaturated air beneath the liquid layer (Fig. 1a). Here – and throughout the manuscript – we show the original mass SCF from the model as a reference for several reasons: the cloud water content characterizes the presence of clouds in a more general way than cloud fraction, it is routinely used as a metric for cloud phase study in the literature (e.g., Cesana et al., 2015; McCoy et al., 2015; Tsushima et al., 2006) and it is also used as an input to compute the simulator cloud phase diagnostics (Section 2.2; Chepfer et al., 2008). Where the mass SCF is greater or near 50%, the lidar simulator only detects liquid-bearing clouds because the much greater total cross-sectional area of the water droplets dominates the lidar returns (Fig. 1b-c). However, as the ice cloud water loading and cloud fraction increase, the lidar simulator classifies more undefined-phase clouds, which are comprised of both liquid and ice particles (Supplementary Fig. S1g-k). Including precipitation in the lidar simulator returns leads to the detection of a substantial extent of hydrometeor thickness directly below the liquid cloud-top layers, and down to the surface (Fig. 1b-c). The second case, an anvil cirrus cloud system at midlatitudes, highlights the substantial impact of frozen precipitation on the lidar simulator returns, which nearly doubles the vertical extent of the lidar ice cloud fraction (Fig. 1e-f), in better agreement with the cloud edges of the native GISS-ModelE3 output (Fig. 1d).

3.2. Global-scale analysis in the ESM configuration

Consistent with the SCM case studies, in global simulations, the addition of precipitation largely increases the lidar cloud fraction (Fig. 2). The changes are mostly attributable to stratiform snow at middle and high levels (heights > 3 km), where most of the ice water path (IWP) resides and obscures some underlying water clouds. In other words, a greater occurrence of middle and high clouds generates more frequent lidar signal attenuation, a shielding effect that prevents the lidar simulator from detecting underlying hydrometeor layers. The magnitude of the total change can be as large as 10 % regionally (in the deep tropics and over the Southern Ocean) and effects extend globally. Stratiform rain also slightly affects the lidar simulator results, although to a much lesser extent (up to 0.4 % absolute), in the tropics and at mid-latitudes. Thus, the lidar simulator is able to detect rain under intermittent conditions, for example, non-turbulent optically thin clouds that do not fully attenuate the lidar signal and produce drizzle as observed over polar regions (Silber et al., 2020). As expected, convective precipitation (Supplementary Fig. S3) has a negligible impact on the simulated lidar returns, since the tops of convective clouds are optically thick and quickly attenuate the lidar signal before it reaches any underlying precipitation. Finally, precipitation has a lesser impact on cloud fraction for those GISS-ModelE3 configurations with a greater high cloud fraction (height > 6.5 km; Supplementary Fig. S4), generating a greater shielding effect that obscures the underlying frozen hydrometeors, and with a greater bias compared to observations (Supplementary Fig. S5).

3.3. Effect of precipitation on cloud phase partitioning

Accounting for precipitation in the CPP substantially changes the relationship between SCF and temperature regardless of whether or not the lidar simulator is used (Fig. 3). The precipitation increases the vertical extent of frozen hydrometeors in the atmosphere substantially more than that of liquid hydrometeors since the volume occupied by frozen hydrometeors in the atmosphere is generally greater than that of liquid hydrometeors (e.g., Fig. 2). As a result, frozen hydrometeors are more likely to be obscured by shielding from overlying cloudy layers, and therefore not detected by the lidar simulator, than their liquid-phase counterparts, which explains the greater difference between the native mass SCF and lidar frequency SCF when precipitation is included. By contrast, when precipitation is ignored, lidar attenuation favors ice detection because the tops of ice clouds are detected by the lidar most of the time whereas lower level water clouds are often obscured by overlying clouds and precipitation (Fig. 3). The impact of the lidar simulator is variable and depends on multiple factors, among which are the amount of shielding by high clouds and the microphysical properties of the precipitation (Supplementary Fig. S6). Thus, for analysis of models with large positive high-level cloud biases, one might consider excluding regimes dominated by high-level clouds when comparing lidar simulator CPP with CALIPSO observations.

Finally, by increasing the amount of ice clouds detected by the simulator, the presence of precipitation yields a more realistic distribution of total cloud amount (Fig. 2) and CPP (Fig. 3) seen by the lidar simulator. For example, without snow, GISS-ModelE3 fails to capture the full vertical extent of ice clouds (Fig. 1e, 2h), which is a common problem in CMIP5 models (Cesana and Waliser, 2016). Additionally, this substantial difference between simulations with and without snow is particularly crucial when evaluating models over the Southern Ocean (SO), where models suffer from large radiative biases (Trenberth and Fasullo, 2010), often linked to a lack of mixed-phase frontal clouds (Bodas-Salcedo et al., 2016) and large intermodel spread in cloud feedbacks (Zelinka et al., 2020). When neglecting precipitation, GISS-ModelE3 consistently underestimates the ice cloud frequency over the SO within the mixed-phase temperature range compared to CALIPSO-GOCCP observations (Supplementary Fig. S7).

3.4. Implications for radiation, cloud feedbacks and climate projections

In addition to modifying the CPP, precipitation substantially impacts radiation. In GISS-ModelE3, adding the effect of large-scale precipitation from the radiation scheme (referred to as precipitation in the remainder of this section), which accounts for nearly all of the impact of precipitation on the lidar simulator, results in offsetting changes in the global average CRE at TOA, with roughly -3 W/m^2 for SW and a similar increase for LW (Supplementary Fig. S8), negligibly changing the net radiative balance at TOA, comparable to the offsetting effect found by Michibata et al. (2020). More importantly, including precipitation substantially increases the global net cloud feedback (Fig. 4a), even doubles it in one configuration (0.21 vs. 0.9 $W\ m^{-2}\ K^{-1}$), quantified using the International Satellite Cloud Climatology Project (ISCCP)-derived radiative kernel method (Zelinka et al., 2016; see also Supplementary text S5). Such a large increase raises possible implications for models' climate sensitivity (Cesana and Del Genio, 2021; Zelinka et al., 2020).

This cloud feedback increase is mostly attributable to the SW component, with a slight offset in the LW. Previous studies showed that a larger amount of frozen hydrometeors relative to all hydrometeors (i.e., a smaller SCF) in an ESM strengthens its negative SW cloud feedback over the SO because more frozen hydrometeors are available to transition to water as climate warms (Tan et al., 2016; Tsushima et al., 2006). Making precipitation visible to the GISS-ModelE3 radiation scheme modestly enhances this negative SW feedback over the SO (Fig. 4a) for two reasons. A smaller decrease in low cloud amount, compared to when precipitation is not seen by radiation, also contributes to a smaller reduction of the negative SW feedback whereas a greater increase in non-low amount (at heights > 3 km) strengthens it. However, the negative SW feedback is substantially reduced on a global scale in GISS-ModelE3 (making it less negative, Fig. 4), attributable to a smaller increase in non-low cloud amount and optical depth seen by the radiation scheme, mostly contributed by the extratropics (Fig. S11). This reduction is particularly large over the Arctic, which could contribute to enhancing the Arctic amplification. While the LW positive feedback is also weakened with snow-aware radiation scheme, the amplitude of the change is far smaller.

On the one hand, the greater amount of non-low clouds in the mean state – contributed by the presence of precipitation – explains the greater altitude feedback in the LW, which quantifies the feedback generated by changes in altitude while keeping the cloud amount and optical depth fixed. On the other hand, the cloud amount and optical depth positive feedbacks are smaller in the LW, which offset the increase from the altitude feedback, because the increase in high-cloud amount and optical depth is smaller when the precipitation is seen by the radiation scheme (Fig. S11).

More generally, the net cloud feedback from cloud above 3 km – where the presence of snow affects the cloud fraction the most – in CMIP5 and CMIP6 models with snow-aware radiation schemes is also greater than that of models without snow-aware radiation schemes (Fig. 4; 0.37 and 0.26 W m^{-2} K^{-1} compared to 0.24 and 0.19 W m^{-2} K^{-1}, respectively). Consistent with our GISS-ModelE3 results, this greater net cloud feedback is attributable to an increase in SW cloud feedback partially offset by a decrease in LW cloud feedback. However, unlike GISS-ModelE3, in CMIP models, changes in the SW are offset by the LW in the extratropics whereas most of the difference originates from the tropics (Fig. 4), mainly for two reasons. First, the net cloud feedback from non-low clouds is negative in both the tropics and the extratropics in GISS-ModelE3 as opposed to being positive in CMIP models, attributable to different responses of clouds to warming (increase or decrease of the cloud amount, see next paragraph), which, in turn, impacts the effect of including the precipitation. Second, the amplitude of GISS-ModelE3 non-low cloud feedback is greater in the extratropics than in the tropics, unlike in CMIP models, which yields a larger change in feedbacks when including precipitation.

Globally, the non-low cloud amount decrease and increase are greater and smaller, respectively, when the precipitation is seen by the radiation scheme, mostly because of stratiform snow. Since stratiform snow is primarily produced by cloud ice, when the ice cloud amount decreases in response to global warming, the stratiform snow generated by these ice clouds is also reduced. As a result, the initial decrease in frozen hydrometeor amount as seen by radiation is further amplified compared to that of cloud ice alone (Fig. S12, 1st column). By contrast, when the non-low cloud amount increases in response to climate warming, some of the cloud ice is replaced by liquid water because of warmer temperatures. These non-low liquid clouds do not produce as much snow as ice clouds, therefore generating a smaller overall increase of the hydrometeor amount seen by radiation compared to that of clouds alone (i.e., without precipitation; Fig. S12, 2nd column). These results, including the increase of net global cloud feedback, remain consistent across all four GISS-ModelE3 configurations (Supplementary Table S2). Moreover, we note that the effect of precipitation on cloud fraction and cloud feedbacks is greatest in those configurations that best match the CALIPSO-GOCCP observations of high-cloud amount and CPP.

4. Conclusions and discussion

Using GISS-ModelE3 simulations and CALIPSO-GOCCP observations, we quantify the effect of precipitation on cloud phase partitioning (CPP) and cloud feedbacks in an ESM, which has not been reported before to our knowledge. To improve consistency between simulations and observations, we modified the widely used and publicly available CALIPSO lidar simulator to include precipitation. Our results indicate that accounting for stratiform frozen precipitation, typically categorized as snow, substantially increases the cloud fraction at middle and high levels (heights > 3 km) and is crucial for faithfully comparing simulated CPP to observations, particularly in the extratropics. Doing so can not only affect global mean SW and LW cloud radiative effects at TOA, but also substantially modify the net cloud feedback – doubling it in one of the four GISS-ModelE3 configurations – with a greater impact over the Arctic.

Yet, previous generation CMIP5 and current generation CMIP6 models typically neglect the radiative effects of snow (J. L. F. Li et al., 2020) (24 out of 27 and 23 out of 37, respectively), similar to our model excursion explored here, and therefore underestimate its net positive contribution to global cloud feedbacks, which may partly explain their smaller average climate sensitivities (3.3 vs. 4.1 K and 3.4 vs. 4.4 K, respectively). All else equal, including this effect in all CMIP6 models would therefore strengthen their net positive cloud feedback from cloud above 3 km (e.g., Fig. 4). It would also further amplify the increase in total net positive cloud feedback between CMIP5 and CMIP6 models (Zelinka et al., 2020), and in turn, the increase in climate sensitivity, which needs to be reconciled with the likelihood that climate sensitivity is already too high in many CMIP6 models(Grégory V. Cesana and Del Genio, 2021; Sherwood et al., 2020; Zhu et al., 2020). Furthermore, adding snow would also decrease SCFs, requiring further ESM tuning to restore the larger initial SCF. As a consequence, a retuned SCF increase (e.g., by either adding liquid clouds or removing ice clouds) is expected to further weaken the negative SW cloud feedback – less cloud ice available to be transformed into more reflective cloud water– and thereby further increase climate sensitivity.

Given the magnitude of impacts on cloud feedbacks and on constraining CPP, we argue that precipitation should be included in ESM radiative transfer and simulator calculations. In addition, we strongly advocate that future ESM development and analysis use a lidar simulator with CALIPSO-GOCCP observations to evaluate both CPP and middle and high-level cloud fractions because they modulate the strength of cloud feedbacks. Systematically characterizing such specific aspects of climate model physics that most impact diversity in future projections is crucial to confidently establishing Earth's rate of warming and climate models as reliable tools going forward.

Acknowledgments

GC and AA were partly supported by a CloudSat-CALIPSO RTOP at the NASA Goddard Institute for Space Studies. IS and GC were supported by DOE grant DE-SC0021004. GC was also supported by NOAA grant NA20OAR4310390. AA, AF and MK were supported by the NASA Modeling, Analysis, and Prediction Program. Contributions of IS and AF were also supported by DOE grant DE-SC0018046. Resources supporting this work were provided by the NASA Center for Climate Simulation (NCCS) at Goddard Space Flight Center.

We thank NASA for providing computing resources to run GISS ESM, NASA and CNES for giving access to CALIPSO observations, and Climserv for giving access to CALIPSO-GOCCP observations and for providing computing resources to run COSP offline. We also acknowledge the World Climate Research Programme's Working Group on Coupled Modeling, which is responsible for CMIP, and thank the climate modeling groups for producing and making available their model output. We also thank Helene Chepfer and Jennifer Kay for useful discussions in generalizing the lidar simulator to include precipitation, Mike Bauer for his preliminary implementation of COSP in GISS-ModelE3 and Mark Zelinka for making his radiative kernels and cloud feedback results publicly available. Finally, we thank Hui Su for editing the manuscript and Takuro Michibata, Yoko Tsushima and the anonymous reviewer for their helpful comments.

Data availability

CALIPSO-GOCCP v2.9 observations (Cesana et al., 2016) were downloaded from the CFMIP-Obs website (http://climserv.ipsl.polytechnique.fr/cfmip-obs/Calipso_goccp.html). The GISS-ModelE3 outputs used to create Figs 1-2-3-4 (Cesana, 2021) are available at zenodo.org via http://doi.org/10.5281/zenodo.4968806. All raw GISS-ModelE3 outputs will be archived at https://portal.nccs.nasa.gov/GISS_modelE/; the final configurations of GISS-ModelE3 will be made part of the CMIP6 model archive. The CMIP cloud feedbacks used inf Fig. 4 are available through Zelinka et al. (2020).

References

Bodas-Salcedo, A., Hill, P. G., Furtado, K., Williams, K. D., Field, P. R., Manners, J. C., et al., (2016), Large contribution of supercooled liquid clouds to the solar radiation budget of the Southern Ocean, *Journal of Climate*, *29*(11), 4213–4228. https://doi.org/10.1175/JCLI-D-15-0564.1

Ceppi, P., Hartmann, D. L., & Webb, M. J., (2016), Mechanisms of the negative shortwave cloud feedback in middle to high latitudes, *Journal of Climate*, *29*(1), 139–157. https://doi.org/10.1175/JCLI-D-15-0327.1

Cesana, G., & Waliser, D. E., (2016), Characterizing and understanding systematic biases in the vertical structure of clouds in CMIP5/CFMIP2 models, *Geophysical Research Letters*, *43*(19), 10,538-10,546. https://doi.org/10.1002/2016GL070515

Cesana, G., Kay, J. E., Chepfer, H., English, J. M., & de Boer, G., (2012), Ubiquitous low-level liquid-containing Arctic clouds: New observations and climate model constraints from CALIPSO-GOCCP, *Geophysical Research Letters*, *39*(20), 1–6. https://doi.org/10.1029/2012GL053385

Cesana, G., Waliser, D. E., Jiang, X., & Li, J. L. F., (2015), Multimodel evaluation of cloud phase transition using satellite and reanalysis data, *Journal of Geophysical Research*, *120*(15), 7871–7892. https://doi.org/10.1002/2014JD022932

Cesana, G., Chepfer, H., Winker, D., Getzewich, B., Cai, X., Jourdan, O., et al., (2016), Using in situ airborne measurements to evaluate three cloud phase products derived from CALIPSO, *Journal of Geophysical Research*, *121*(10), 5788–5808. https://doi.org/10.1002/2015JD024334

Cesana, Gregory, & Storelvmo, T., (2017), Improving climate projections by understanding how cloud phase affects radiation, *Journal of Geophysical Research*, *122*(8), 4594–4599. https://doi.org/10.1002/2017JD026927

Cesana, Grégory, & Chepfer, H., (2013), Evaluation of the cloud thermodynamic phase in a climate model using CALIPSO-GOCCP, *Journal of Geophysical Research: Atmospheres*, *118*(14), 7922–7937. https://doi.org/10.1002/jgrd.50376

Cesana, Grégory, Del Genio, A. D., Ackerman, A. S., Kelley, M., Elsaesser, G., Fridlind, A. M., et al., (2019), Evaluating models' response of tropical low clouds to SST forcings using CALIPSO observations, *Atmospheric Chemistry and Physics*, *19*(5), 2813–2832. https://doi.org/10.5194/acp-19-2813-2019

Cesana, Grégory V., & Del Genio, A. D., (2021), Observational constraint on cloud feedbacks suggests moderate climate sensitivity, *Nature Climate Change*, *11*(3), 213–218. https://doi.org/10.1038/s41558-020-00970-y

Chepfer, H., Chiriaco, M., Vautard, R., & Spinhirne, J., (2007), Evaluation of MM5 optically thin clouds over Europe in fall using ICESat lidar spaceborne observations, *Monthly Weather Review*, *135*(7), 2737–2753. https://doi.org/10.1175/MWR3413.1

Chepfer, H., Bony, S., Winker, D., Chiriaco, M., Dufresne, J.-L., & Sèze, G., (2008), Use of CALIPSO lidar observations to evaluate the cloudiness simulated by a climate model, *Geophysical Research Letters*, *35*(15), L15704. https://doi.org/10.1029/2008GL034207

Danabasoglu, G., Lamarque, J. F., Bacmeister, J., Bailey, D. A., DuVivier, A. K., Edwards, J., et al., (2020), The Community Earth System Model Version 2 (CESM2), *Journal of Advances in Modeling Earth Systems*, *12*(2), 1–35. https://doi.org/10.1029/2019MS001916

DeMott, P. J., Prenni, A. J., Liu, X., Kreidenweis, S. M., Petters, M. D., Twohy, C. H., et al., (2010), Predicting global atmospheric ice nuclei distributions and their impacts on climate, *Proceedings of the National Academy of Sciences of the United States of America*, *107*(25), 11217–11222. https://doi.org/10.1073/pnas.0910818107

Foot, J. S., (1988), Some observations of the optical properties of clouds. II: Cirrus, *Quarterly Journal of the Royal Meteorological Society*, *114*(479), 145–164. https://doi.org/10.1002/qj.49711447908

Gettelman, A., & Morrison, H., (2015), Advanced two-moment bulk microphysics for global models. Part I: Off-line tests and comparison with other schemes, *Journal of Climate*, *28*(3), 1268–1287. https://doi.org/10.1175/JCLI-D-14-00102.1

Golaz, J. C., Caldwell, P. M., Van Roekel, L. P., Petersen, M. R., Tang, Q., Wolfe, J. D., et al., (2019), The DOE E3SM Coupled Model Version 1: Overview and Evaluation at Standard Resolution, *Journal of Advances in Modeling Earth Systems*, *11*(7), 2089–2129. https://doi.org/10.1029/2018MS001603

Hu, Y., Winker, D., Vaughan, M., Lin, B., Omar, A., Trepte, C., et al., (2009), CALIPSO/CALIOP cloud phase discrimination algorithm, *Journal of Atmospheric and Oceanic Technology*, *26*(11), 2293–2309. https://doi.org/10.1175/2009JTECHA1280.1

Kawai, H., Yukimoto, S., Koshiro, T., Oshima, N., Tanaka, T., Yoshimura, H., & Nagasawa, R., (2019), Significant improvement of cloud representation in the global climate model MRI-ESM2, *Geoscientific Model Development*, *12*(7), 2875–2897. https://doi.org/10.5194/gmd-12-2875-2019

Kay, J. E., Wall, C., Yettella, V., Medeiros, B., Hannay, C., Caldwell, P., & Bitz, C., (2016), No access global climate impacts of fixing the Southern Ocean shortwave radiation bias in the Community Earth System Model (CESM), *Journal of Climate*, *29*(12), 4617–4636. https://doi.org/10.1175/JCLI-D-15-0358.1

Klein, S. A., McCoy, R. B., Morrison, H., Ackerman, A. S., Avramov, A., Boer, G. de, et al., (2009), Intercomparison of model simulations of mixed-phase clouds observed during the ARM Mixed-Phase Arctic Cloud Experiment. I: single-layer cloud, *Quarterly Journal of the Royal Meteorological Society*, *135*(641), 979–1002. https://doi.org/10.1002/qj.416

Komurcu, M., Storelvmo, T., Tan, I., Lohmann, U., Yun, Y., Penner, J. E., et al., (2014), Intercomparison of the cloud water phase among global climate models, *Journal of Geophysical Research: Atmospheres*, *119*(6), 3372–3400. https://doi.org/10.1002/2013JD021119

Korolev, A., (2007), Limitations of the Wegener–Bergeron–Findeisen Mechanism in the Evolution of Mixed-Phase Clouds, *Journal of the Atmospheric Sciences*, *64*(9), 3372–3375. https://doi.org/10.1175/jas4035.1

Li, J.-L. F., Forbes, R. M., Waliser, D. E., Stephens, G., & Lee, S., (2014), Characterizing the radiative impacts of precipitating snow in the ECMWF Integrated Forecast System global model, *Journal of Geophysical Research: Atmospheres*, *119*(16), 9626–9637. https://doi.org/10.1002/2014JD021450

Li, J.-L. F., Lee, W.-L., Waliser, D. E., Stachnik, J. P., Fetzer, E., Wong, S., & Yue, Q., (2014), Characterizing tropical Pacific water vapor and radiative biases in CMIP5 GCMs: Observation-based analyses and a snow and radiation interaction sensitivity experiment, *Journal of Geophysical Research: Atmospheres*, *119*(19), 10,981-10,995. https://doi.org/10.1002/2014JD021924

Li, J. L. F., Xu, K. M., Jiang, J. H., Lee, W. L., Wang, L. C., Yu, J. Y., et al., (2020), An Overview of CMIP5 and CMIP6 Simulated Cloud Ice, Radiation Fields, Surface Wind Stress, Sea Surface Temperatures, and Precipitation Over Tropical and Subtropical Oceans, *Journal of Geophysical Research: Atmospheres*, *125*(15), 5–10. https://doi.org/10.1029/2020JD032848

Madeleine, J. B., Hourdin, F., Grandpeix, J. Y., Rio, C., Dufresne, J. L., Vignon, E., et al., (2020), Improved Representation of Clouds in the Atmospheric Component LMDZ6A of the IPSL-CM6A Earth System Model, *Journal of Advances in Modeling Earth Systems*, *12*(10). https://doi.org/10.1029/2020MS002046

McCoy, D. T., Hartmann, D. L., Zelinka, M. D., Ceppi, P., & Grosvenor, D. P., (2015), Mixed-phase cloud physics and Southern Ocean cloud feedback in climate models, *Journal of Geophysical Research*, *120*(18), 9539–9554. https://doi.org/10.1002/2015JD023603

Michibata, T., Suzuki, K., & Takemura, T., (2020), Snow-induced buffering in aerosol-cloud interactions, *Atmospheric Chemistry and Physics*, *20*(22), 13771–13780. https://doi.org/10.5194/acp-20-13771-2020

Mitchell, J. F. B., Senior, C. A., & Ingram, W. J., (1989), C02 and climate: a missing feedback?, *Nature*, *341*(6238), 132–134. https://doi.org/10.1038/341132a0

Muhlbauer, A., Kalesse, H., & Kollias, P., (2014), Vertical velocities and turbulence in midlatitude anvil cirrus: A comparison between in situ aircraft measurements and ground-based Doppler cloud radar retrievals, *Geophysical Research Letters*, *41*(22), 7814–7821. https://doi.org/10.1002/2014GL062279

Mülmenstädt, J., Salzmann, M., Kay, J. E., Zelinka, M. D., Ma, P. L., Nam, C., et al., (2021), An underestimated negative cloud feedback from cloud lifetime changes, *Nature Climate Change*, *11*(6), 508–513. https://doi.org/10.1038/s41558-021-01038-1

Quaas, J., (2004), Evaluation of cloud thermodynamic phase parametrizations in the LMDZ GCM by using POLDER satellite data, *31*, 1–5. https://doi.org/10.1029/2003GL019095

Rangno, A. L., & Hobbs, P. V., (2001), Ice particles in stratiform clouds in the Arctic and possible mechanisms for the production of high ice concentrations, *Journal of Geophysical Research Atmospheres*, *106*(D14), 15065–15075. https://doi.org/10.1029/2000JD900286

Ringer, M. a, Andrews, T., & Webb, M. J., (2014), Ocean Climate Change Experiments, *5*(ii), 1–8. https://doi.org/10.1002/2014GL060347.Received

Senior, C. A., & Mitchell, J. F. B., (1993), Carbon Dioxide and Climate. The Impact of Cloud Parameterization, *Journal of Climate*, *6*(3), 393–418. https://doi.org/10.1175/1520-0442(1993)006<0393:CDACTI>2.0.CO;2

Sherwood, S. C., Webb, M. J., Annan, J. D., Armour, K. C., Forster, P. M., Hargreaves, J. C., et al., (2020), An Assessment of Earth's Climate Sensitivity Using Multiple Lines of Evidence, *Reviews of Geophysics*, *58*(4), 1–92. https://doi.org/10.1029/2019RG000678

Silber, I., Fridlind, A. M., Verlinde, J., Ackerman, A. S., Chen, Y. S., Bromwich, D. H., et al., (2019), Persistent Supercooled Drizzle at Temperatures Below −25 °C Observed at McMurdo Station, Antarctica, *Journal of Geophysical Research: Atmospheres*, *124*(20), 10878–10895. https://doi.org/10.1029/2019JD030882

Silber, I., Fridlind, A. M., Verlinde, J., Russell, L. M., & Ackerman, A. S., (2020), Nonturbulent Liquid-Bearing Polar Clouds: Observed Frequency of Occurrence and Simulated Sensitivity to Gravity Waves, *Geophysical Research Letters*, *47*(10), 1–11. https://doi.org/10.1029/2020GL087099

Silber, I., Fridlind, A., Verlinde, J., Ackerman, A., Cesana, G., & Knopf, D., (2020), The Prevalence of Precipitation from Polar Supercooled Clouds, *Atmospheric Chemistry and Physics Discussions*, (October), 1–32. https://doi.org/10.5194/acp-2020-993

Smith, R. N. B., (1990), A scheme for predicting layer clouds and their water content in a general circulation model, *Quarterly Journal of the Royal Meteorological Society*, *116*(492), 435–460. https://doi.org/10.1002/qj.49711649210

Tan, I., Storelvmo, T., & Zelinka, M. D., (2016), Observational constraints on mixed-phase clouds imply higher climate sensitivity, *Science*, *352*(6282), 224–227. https://doi.org/10.1126/science.aad5300

Trenberth, K. E., & Fasullo, J. T., (2010), Simulation of present-day and twenty-first-century energy budgets of the southern oceans, *Journal of Climate*, *23*(2), 440–454. https://doi.org/10.1175/2009JCLI3152.1

Tsushima, Y., Emori, S., Ogura, T., Kimoto, M., Webb, M. J., Williams, K. D., et al., (2006), Importance of the mixed-phase cloud distribution in the control climate for assessing the response of clouds to carbon dioxide increase: A multi-model study, *Climate Dynamics*, *27*(2–3), 113–126. https://doi.org/10.1007/s00382-006-0127-7

Webb, M. J., Andrews, T., Bodas-Salcedo, A., Bony, S., Bretherton, C. S., Chadwick, R., et al., (2017), The Cloud Feedback Model Intercomparison Project (CFMIP) contribution to CMIP6, *Geoscientific Model Development*, *10*(1), 359–384. https://doi.org/10.5194/gmd-10-359-2017

Wilson, D. R., & Ballard, S. P., (1999), A microphysically based precipitation scheme for the UK meteorological office unified model, *Quarterly Journal of the Royal Meteorological Society*, *125*(557), 1607–1636. https://doi.org/10.1002/qj.49712555707

Yoshida, R., Okamoto, H., Hagihara, Y., & Ishimoto, H., (2010), Global analysis of cloud phase and ice crystal orientation from Cloud-Aerosol Lidar and Infrared Pathfinder Satellite Observation (CALIPSO) data using attenuated backscattering and depolarization ratio, *Journal of Geophysical Research Atmospheres*, *115*(16), 1–12. https://doi.org/10.1029/2009JD012334

Zelinka, M. D., Klein, S. A., & Hartmann, D. L., (2012a), Computing and Partitioning Cloud Feedbacks Using Cloud Property Histograms. Part I: Cloud Radiative Kernels, *Journal of Climate*, *25*(11), 3715–3735. https://doi.org/10.1175/jcli-d-11-00248.1

Zelinka, M. D., Klein, S. A., & Hartmann, D. L., (2012b), Computing and partitioning cloud feedbacks using cloud property histograms. Part II: Attribution to changes in cloud amount, altitude, and optical depth, *Journal of Climate*, *25*(11), 3736–3754. https://doi.org/10.1175/JCLI-D-11-00249.1

Zelinka, M. D., Zhou, C., & Klein, S. A., (2016), Insights from a refined decomposition of cloud feedbacks, *Geophysical Research Letters*, *43*(17), 9259–9269. https://doi.org/10.1002/2016GL069917

Zelinka, M. D., Myers, T. A., McCoy, D. T., Po-Chedley, S., Caldwell, P. M., Ceppi, P., et al., (2020), Causes of Higher Climate Sensitivity in CMIP6 Models, *Geophysical Research Letters*, *47*(1), 1–12. https://doi.org/10.1029/2019GL085782

Zhang, Y., Xie, S., Lin, W., Klein, S. A., Zelinka, M., Ma, P. L., et al., (2019), Evaluation of Clouds in Version 1 of the E3SM Atmosphere Model With Satellite Simulators, *Journal of Advances in Modeling Earth Systems*, *11*(5), 1253–1268. https://doi.org/10.1029/2018MS001562

Zhu, J., Poulsen, C. J., & Otto-Bliesner, B. L., (2020), High climate sensitivity in CMIP6 model not supported by paleoclimate, *Nature Climate Change*, *10*(5), 378–379. https://doi.org/10.1038/s41558-020-0764-6

Figures

Figure 1: Evaluation of the effect of precipitation on the lidar simulator. Cloud phase partitioning profiles in two case studies: Liquid-topped mixed-phase cloud in the Antarctic (left column) and stratiform cirrus case over the US Southern Great Plains (right column) as a function of the time. The top row (a, d) correspond to the mass SCF defined as liquid/(ice+liquid) water content from the native GISS-ModelE3 outputs. The middle and bottom rows show the frequency SCF computed as the liquid/(ice+liquid) cloud frequency from the lidar simulator GISS-ModelE3 outputs (b, e) without and (c, f) with precipitation outputs, respectively. See Supplementary text S4 and Figs S1 and S2 for more details about the setup of the case studies.

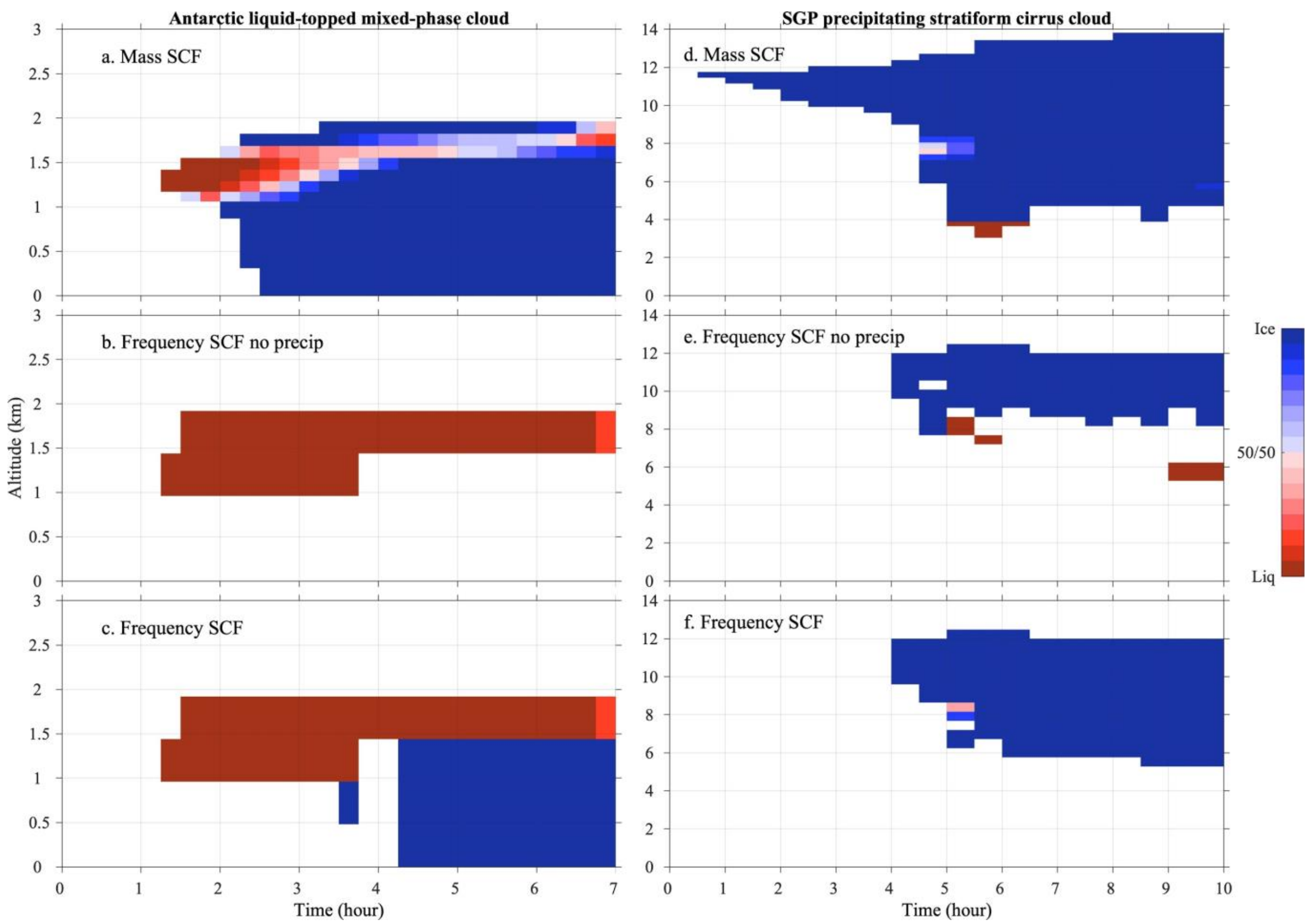

Figure 2: Effect of the precipitation on cloud phase fraction profiles. Zonal profiles of all (first column), ice (second column) and liquid (third column) cloud fraction (%) for CALIPSO-GOCCP (2007-2016 Nighttime v2.9, first row) and the lidar simulator GISS-ModelE3 outputs with precipitation (second row, *Precip*), without precipitation (third row, *No precip*) and the difference between *Precip* and *No precip* (fourth row). Note that most of the change is attributed to stratiform snow. Note that the zonal mean of simulator total cloud fraction and ice and liquid water paths are shown in Supplementary Figure S10.

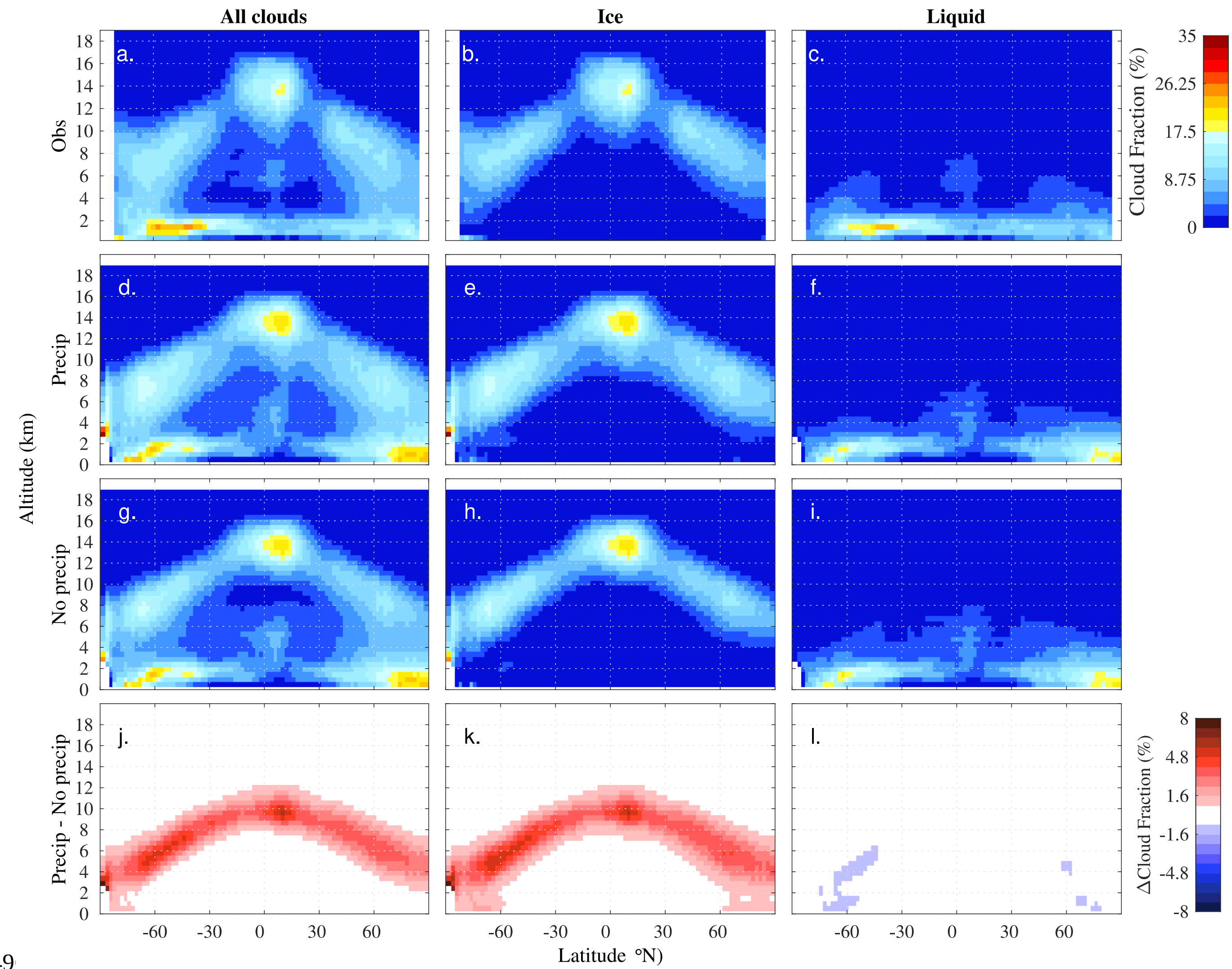

Figure 3: Effect of the precipitation on the relation between mass or frequency supercooled cloud fraction and temperature. The figure emphasizes the difference between mass (dashed lines) and frequency (solid lines) SCF with (blue) and without (cyan) the effect of precipitation in GISS-ModelE3 compared to the CALIPSO-GOCCP observations frequency SCF (black line, 2007-2016 Nighttime v2.9) as a function of temperature (°C). Note that the lidar simulator is used to obtain the frequency SCF in GISS-ModelE3. The shaded areas correspond to uncertainty estimates (see text S1 for details).

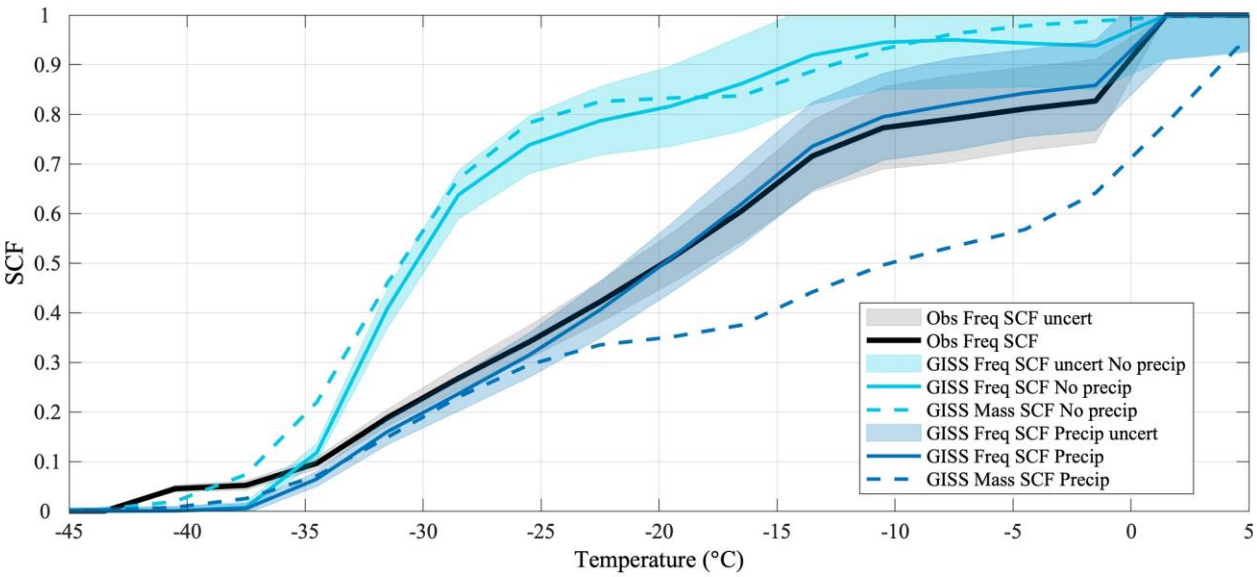

Figure 4: Effect of precipitation on cloud feedbacks. Zonal (left) and global (right) mean of total cloud feedbacks (W m^{-2} K^{-1}, a-b) and their separate contributions from non-low (at pressures ≤ 680 hPa, c-d) and low (at pressures > 680 hPa, e-f) clouds for GISS-ModelE3 simulations with (solid line, *Precip*) and without (dotted line, *No LS precip*) the effect of large-scale precipitation. The two bottom rows correspond to cloud feedbacks from non-low clouds for the CMIP6 (g-h) and CMIP5 (i-j) models (listed in Supplementary Table S3) with and without snow-aware radiation schemes. The net, LW and SW cloud feedbacks correspond to the black, red and blue lines, respectively. The definition of cloud feedbacks is given in Supplementary text S5 and further decomposition by cloud feedback types for GISS-ModelE3 is shown in Supplementary Fig. S11 and global averages in Supplementary Table S1-2.

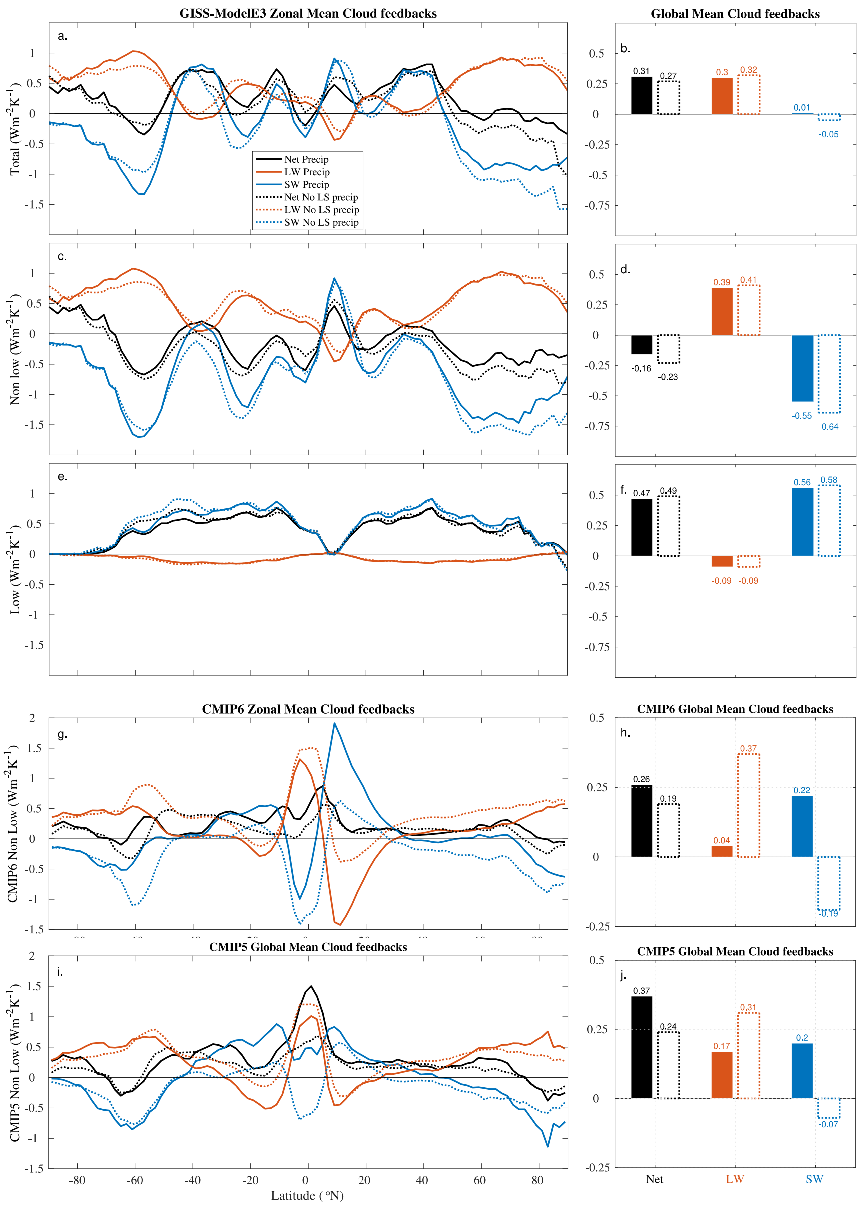

Figure 1.

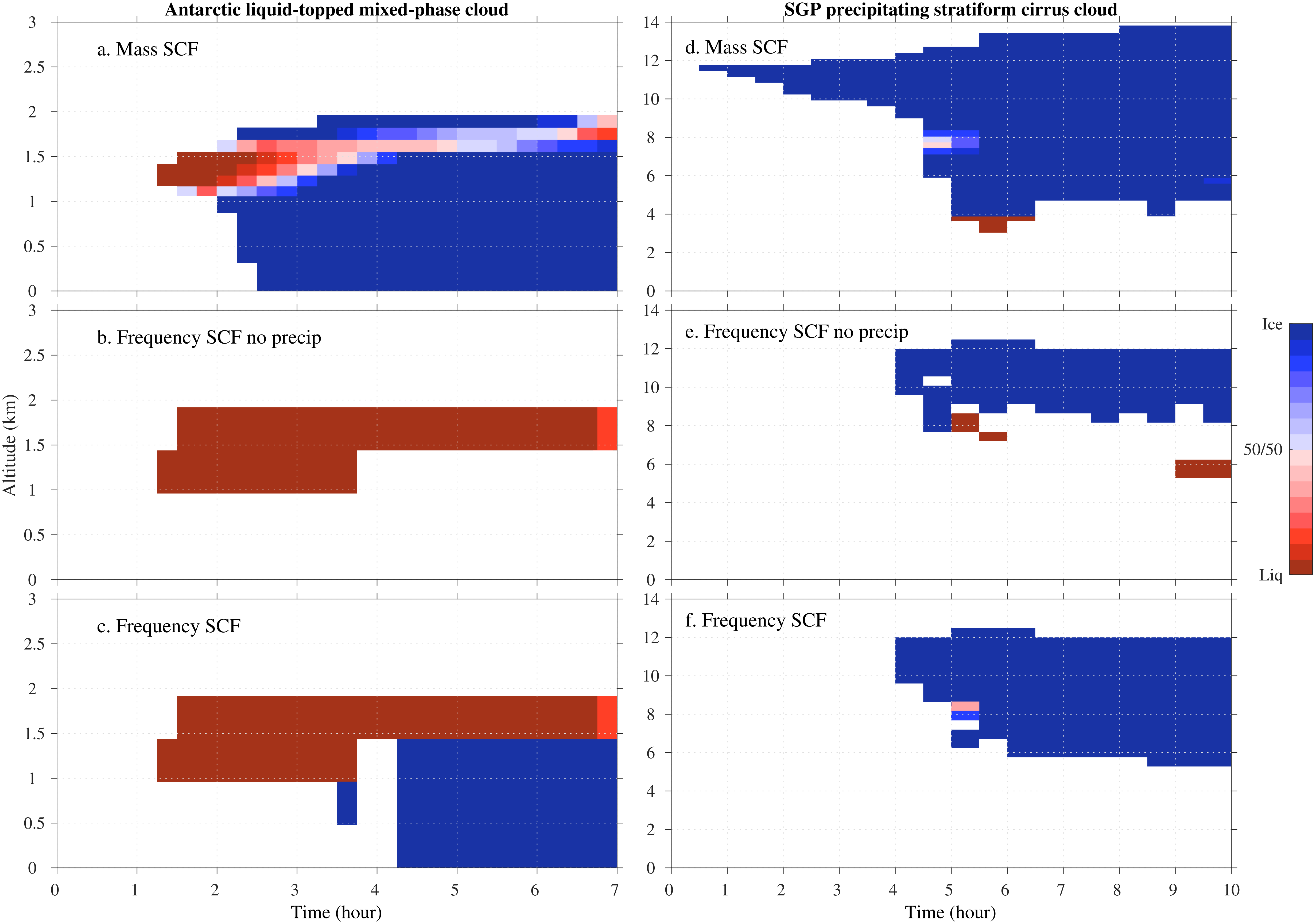

Antarctic liquid-topped mixed-phase cloud
SGP precipitating stratiform cirrus cloud
a. Mass SCF
b. Frequency SCF no precip
c. Frequency SCF
d. Mass SCF
e. Frequency SCF no precip
f. Frequency SCF
Altitude (km)
Time (hour)
Ice
50/50
Liq

Figure 2.

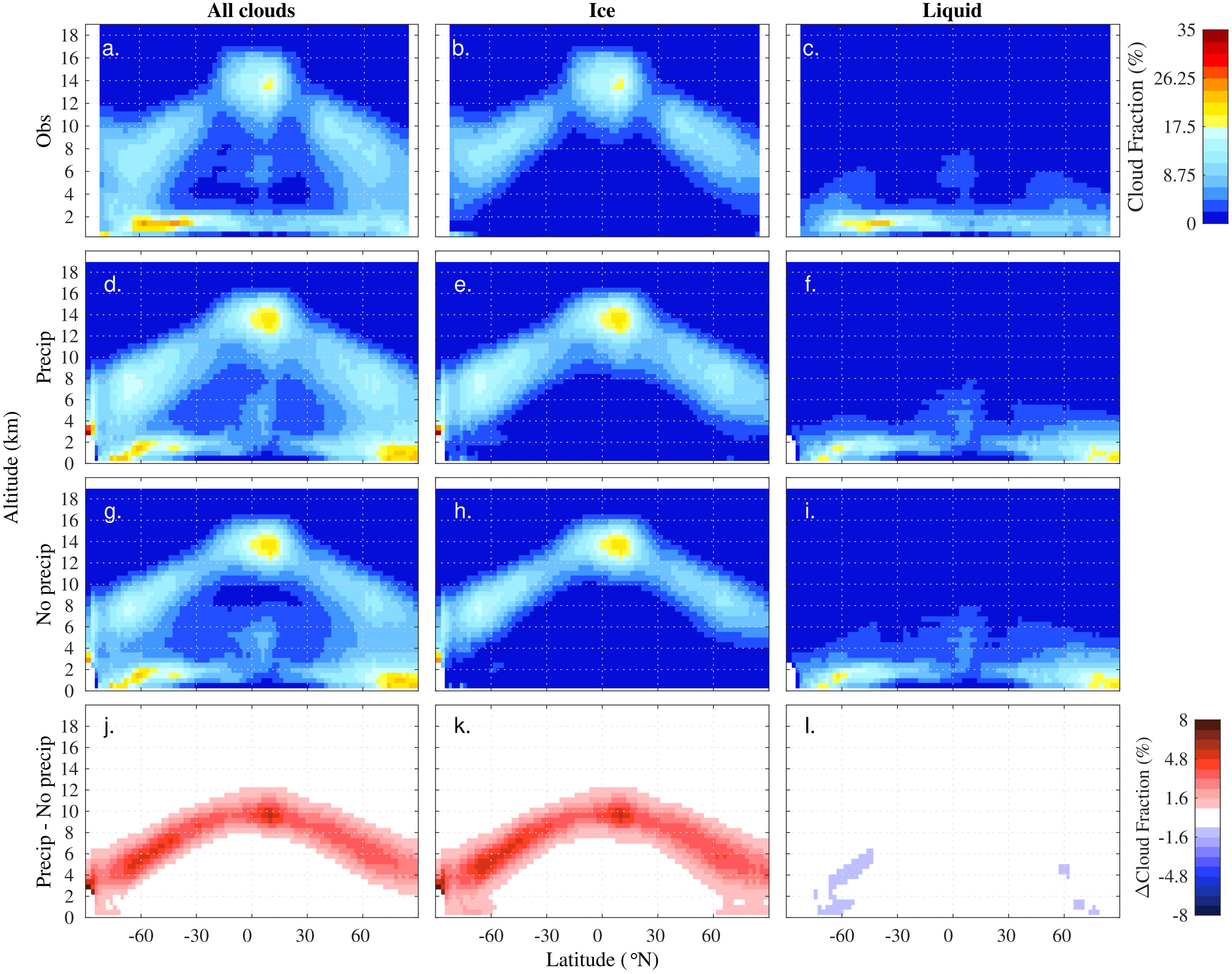

All clouds
Ice
Liquid
Obs
Precip
No precip
Precip - No precip
Altitude (km)
Latitude (°N)
Cloud Fraction (%)
35
26.25
17.5
8.75
0
ΔCloud Fraction (%)
8
4.8
1.6
-1.6
-4.8
-8
a.
b.
c.
d.
e.
f.
g.
h.
i.
j.
k.
l.
18
16
14
12
10
8
6
4
2
0
-60
-30
0
30
60

Figure 3.

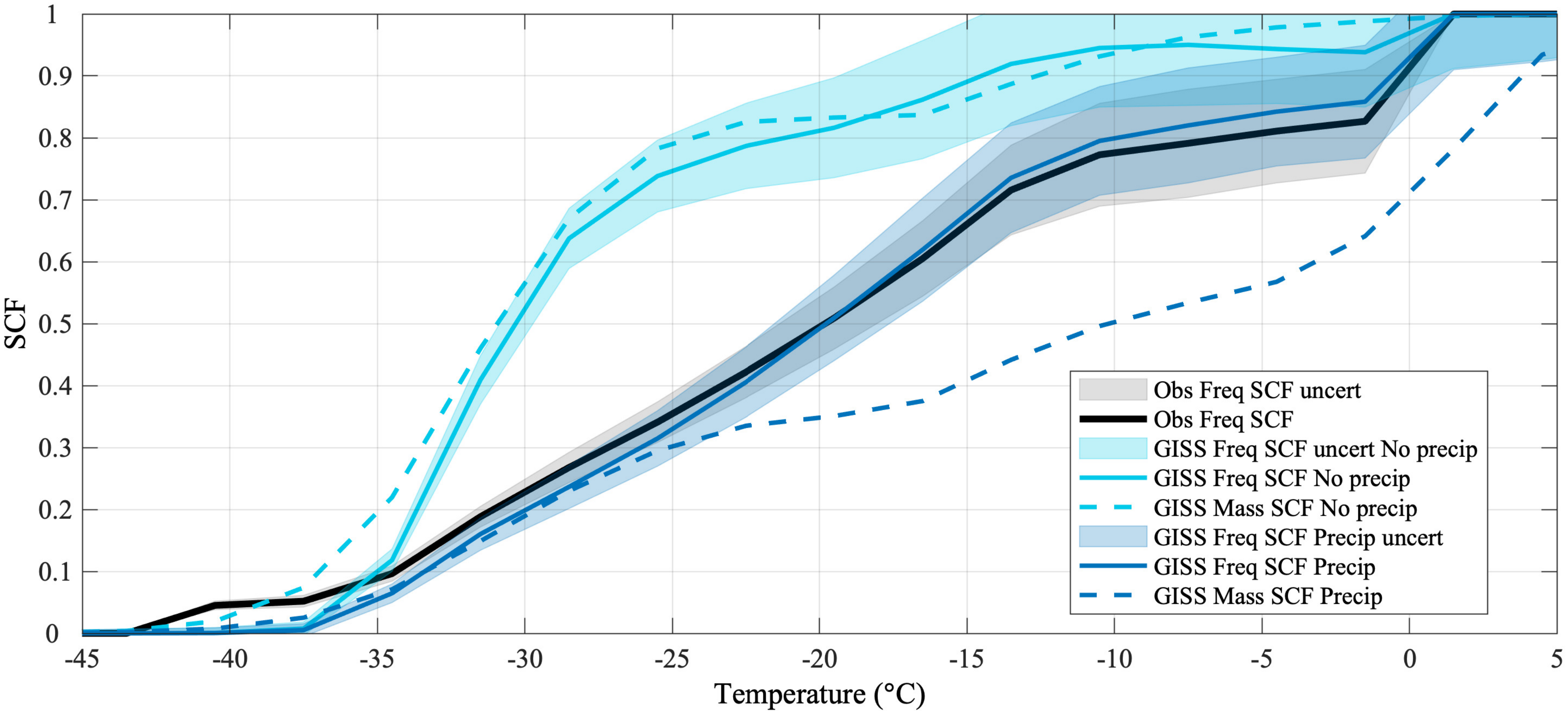

SCF
Temperature (°C)
1
0.9
0.8
0.7
0.6
0.5
0.4
0.3
0.2
0.1
0
-45
-40
-35
-30
-25
-20
-15
-10
-5
0
5
Obs Freq SCF uncert
Obs Freq SCF
GISS Freq SCF uncert No precip
GISS Freq SCF No precip
GISS Mass SCF No precip
GISS Freq SCF Precip uncert
GISS Freq SCF Precip
GISS Mass SCF Precip

Figure 4.

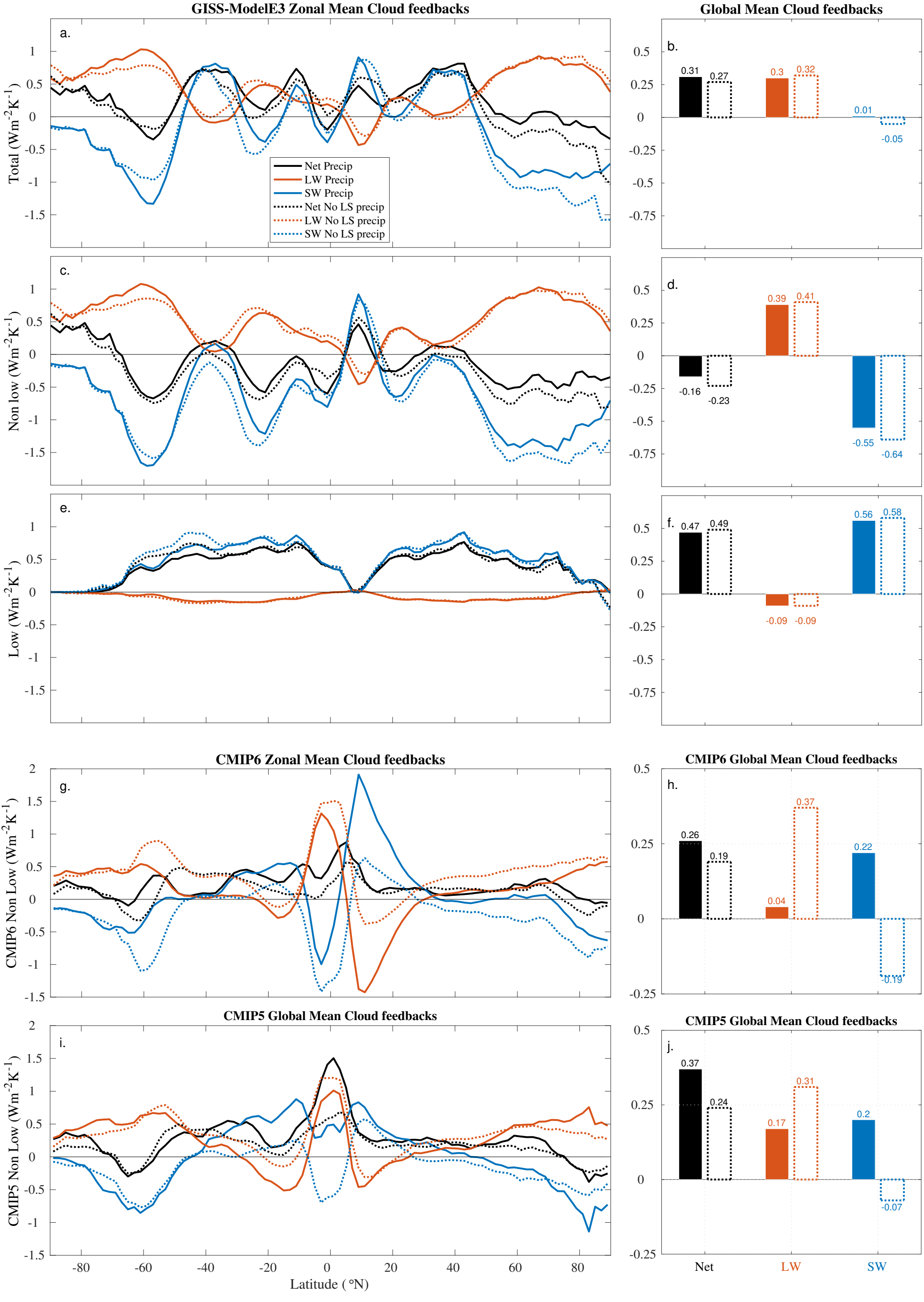

GISS-ModelE3 Zonal Mean Cloud feedbacks
Global Mean Cloud feedbacks
a.
b.
c.
d.
e.
f.
Total ($Wm^{-2}K^{-1}$)
Non low ($Wm^{-2}K^{-1}$)
Low ($Wm^{-2}K^{-1}$)
Net Precip
LW Precip
SW Precip
Net No LS precip
LW No LS precip
SW No LS precip
0.31
0.27
0.3
0.32
0.01
-0.05
-0.16
-0.23
0.39
0.41
-0.55
-0.64
0.47
0.49
-0.09
-0.09
0.56
0.58
CMIP6 Zonal Mean Cloud feedbacks
CMIP6 Global Mean Cloud feedbacks
g.
h.
CMIP6 Non Low ($Wm^{-2}K^{-1}$)
0.26
0.19
0.04
0.37
0.22
-0.19
CMIP5 Global Mean Cloud feedbacks
CMIP5 Global Mean Cloud feedbacks
i.
j.
CMIP5 Non Low ($Wm^{-2}K^{-1}$)
0.37
0.24
0.17
0.31
0.2
-0.07
Latitude (°N)
Net
LW
SW